

Initial Correlations and Time-Retarded Noise in Dynamical Decoupling Schemes for Superconducting Qubits

Kiyoto Nakamura^{1,*} and Joachim Ankerhold¹

¹*Institute for Complex Quantum Systems and IQST, Ulm University, D-89069 Ulm, Germany*

(Dated: August 29, 2024)

One of the simplest and least resource-intensive methods to suppress decoherence for superconducting qubit operations, namely, dynamical decoupling (DD), is investigated for a broad range of realistic noise sources with time-retarded feedback. By way of example, the Carr–Purcell–Meiboom–Gill (CPMG) sequence is analyzed in a numerically rigorous manner accounting also for correlations between qubit and environment. Since experimentally noise sources are characterized through spectral densities, we adopt the spin–boson model as a suitable platform to describe the qubit dynamics under DD for a given spectral density $J(\omega) \propto \omega^s$. To cover a broad range of noise sources, the spectral exponent s is varied from $s = 1$ (Ohmic bath) to a substantially small value $0 < s \ll 1$ (deep sub-Ohmic bath), in order to investigate the impact of time-nonlocal back action on DD performances for enhanced coherence times. As reference to the DD schemes, dynamics of a single qubit subject to Ramsey sequences without any pulses and Hahn echo (HE) sequences are also investigated.

I. INTRODUCTION

While remarkable progress in quantum computing has been made in the last decade [1–8], decoherence remains one of the main obstacles to further improvement. During an idle phase in a quantum algorithm, in which certain qubits are left without any control to wait the completion of manipulation of other qubits, quantum states of qubits must be conserved for subsequent calculations. However, those quantum states, especially coherent superpositions, are easily destroyed by environmental noise, which is referred to as decoherence. Suppression of decoherence hence directly leads to improvements of quantum computation. In addition to the coherence time during an idle phase (quantum memory) mentioned above, gate operations are affected by decoherence. During pulse applications, a qubit state starts to deviate from a desired state because of decoherence, which leads to a mismatch of rotation angles and axes.

In order to guide circuit designs and advanced pulse shaping, numerical simulations based on proper noise models are indispensable. The most powerful framework is provided by system–reservoir models (or more specifically, the spin–boson model) [9] which has begun to be used to characterize decoherence properties and gate fidelities beyond standard weak coupling treatments [10–16]. The model is advantageous because information about environmental noise is completely encoded in the spectral noise power, which can be experimentally obtained, for example, via noise spectroscopy [17–19] and characterization of quasiparticle noise in superconducting qubits [20–22].

To further improve the capability of quantum computations, characterization of noise sources can only be the first step: Quantum control techniques based on this

knowledge must be implemented and eventually quantum error correction for multi-qubit architectures using syndrome qubits are the ultimate goal. For gate operations, pulse shaping techniques based on optimal control theory [23] have been proposed. A numerical study [24] for system–reservoir models in which the reservoir dynamics is treated in a numerically rigorous manner has already been conducted, disclosing non-Markovian effects beyond the rotating wave approximation.

For the improvement of coherence times, the dynamical decoupling (DD) scheme [25] is one of the most widely used technique owing to its simplicity of the implementation. Originating from techniques for nuclear magnetic resonance (NMR) [26, 27], in which the Hahn echo (HE) sequence [28] is repeated, a wide variety of DD schemes has been theoretically proposed. Examples include schemes to suppress noise caused by arbitrary couplings to an environment [29, 30], higher-order contributions of the noise in terms of pulse intervals [31, 32], and errors arising during applications of pulses with finite widths [33]. Their performances have been tested experimentally [34] in comparison with numerical predictions [35, 36] for different schemes. In some experiments, the dependence of the performance on different quantum devices has been investigated [37, 38]. DD schemes with optimization processes for pulse intervals and rotation axes have also been proposed [39–41].

In contrast to this impressive body of literature, DD schemes in presence of experimentally realistic noise sources have not been analyzed in an elaborate manner. This seems to be due to the fact that the aim of DD schemes is to universally suppress the undesired time evolution of the system induced by interactions between the qubit system and environment without any knowledge of the coupling forms. A few examples for specific open systems include studies in which the standard Ohmic [25, 32] or $1/f$ noise [35, 42] are considered. However, a comparison between different types of noise sources including the omnipresent $1/f^\varepsilon$ -type noise ($\varepsilon \neq 1$) as a major noise source

* kiyoto.nakamura@uni-ulm.de

for transmon qubits [17, 43] has not been presented yet in a comprehensive manner.

Considering that the DD performance actually depends on the qubit devices [37, 38], an analysis across a broad range of spectral noise powers is essential. In addition, it is assumed in most of the previous studies that the time interval between two pulses is sufficiently short compared to typical timescales of the environment. However, this is in contrast to typical experimental situations, where the lengths of pulses for state-of-the-art transmon qubits are much longer. Another key assumption imposed in previous studies is the factorized initial states between the system and reservoir: This assumption is valid only in the weak system–reservoir coupling limit, which does not hold for a lot of qubit systems. Two questions thus arise: What is the performance of DD schemes beyond the short-time assumption for various noise sources? What is the impact of initial correlations between qubit and environment? In this paper we provide such an analysis that is expected to be beneficial for current noisy intermediate-scale quantum (NISQ) devices, in particular, in presence of realistic noise sources with time-retarded feedback.

For this purpose, we employ a rigorous treatment that does not suffer from any assumption about weak coupling and timescale separation (Born-Markov approximation). More specifically and consistent with previous studies for gate performance [16], we provide predictions for performances of Ramsey experiments without pulses, of HE sequences, and of DD schemes. To focus on the impact of quantum noise, we restrict ourselves to one of the simplest sequences, that is, the Carr–Purcell–Meiboom–Gill (CPMG) sequence [26, 27] with impulsive pulses (bang-bang control) for the pure dephasing case. For these schemes, a broad class of thermal reservoirs relevant for superconducting qubits ranging from reservoirs with Ohmic to those with deep sub-Ohmic characteristics is adopted. For DD protocols, parameters such as the idle times between two consecutive pulses are tuned over a wide interval from being much shorter to being much longer compared to qubit timescales, in order to guide control schemes for practical NISQ devices. To better understand the global characteristics of the DD performance, which is defined by the coherence time, we also look into details of the local dynamics of the qubit system.

This paper is organized as follows. In Sec. II, we briefly introduce the spin–boson model and discuss parameter values for the subsequent numerical calculations. Since we only consider pure dephasing in this paper, analytical expression for dynamics of a single qubit is derived. Section III is devoted to numerical results. Before we investigate the DD performance, we discuss the Ramsey experiments without DD pulses and simpler HE sequences as reference. In Sec. III A, contribution of static correlation between the system and reservoir at an initial time as well as the profile of the spectral noise power to qubit dynamics is explored. HE experiments with various spec-

tral noise powers and pulse intervals are investigated in Sec. III B. Finally, the DD performance for a broad class of the reservoir and a wide range of duration is analyzed in Sec. III C. We make concluding remarks in Sec. IV.

II. MODEL AND METHOD

In this paper, we consider a single qubit affected by quantum Gaussian noise. The total Hamiltonian reads

$$\hat{H}_{\text{tot}} = \frac{\hbar\omega_q}{2}\hat{\sigma}_z - \hbar\hat{\sigma}_z\hat{X} + \hat{H}_R = \hat{H}_S - \hat{V}\hat{X} + \hat{H}_R. \quad (1)$$

Here, the single qubit has been approximated as a two level system, and $\hat{\sigma}_\alpha$ ($\alpha \in \{x, y, z\}$) is the Pauli matrix. The noise effects are taken into account as the dynamics of a reservoir consisting of an infinite number of harmonic oscillators. The qubit frequency is given by ω_q in Eq. (1), and \hat{H}_R is the Hamiltonian of the reservoir.

The coupling between the qubit system and reservoir is in the bilinear form, $\hat{V}\hat{X}$, where $\hat{V} = \hbar\hat{\sigma}_z$ is the system part and \hat{X} is the reservoir part. Note that we adopt the pure-dephasing coupling for the simplicity. Considering that the population-relaxation time is much longer than the coherence time in a lot of qubit devices, the above form for \hat{V} might be plausible approximation. The reservoir is characterized by the autocorrelation function $C(t) = \text{tr}\{\hat{X}(t)\hat{X}(0)\hat{\rho}_{R,\text{eq}}\}$, where $\hat{\rho}_{R,\text{eq}}$ is the Boltzmann distribution of the reservoir, $\hat{\rho}_{R,\text{eq}} = e^{-\beta\hat{H}_R}/\text{tr}\{e^{-\beta\hat{H}_R}\}$ ($\beta = 1/k_B T$ is the inverse temperature with the Boltzmann constant k_B). More specifically, we introduce the spectral density

$$J(\omega) = \frac{1 - e^{-\beta\hbar\omega}}{\hbar} S_\beta(\omega) = \frac{1 - e^{-\beta\hbar\omega}}{2\pi\hbar} \int_{-\infty}^{\infty} dt C(t) e^{i\omega t},$$

and the reservoir is characterized through the parameters of $J(\omega)$. Here, $S_\beta(\omega)$ is the spectral noise power.

To express the sequence of the HE and DD simply, we define the following superoperators: the rotation superoperator of the system on the Bloch sphere,

$$\mathcal{R}_x \hat{\rho}_{\text{tot}}(t) = \hat{R}_x(\pi) \rho_{\text{tot}}(t) \hat{R}_x(-\pi), \quad (2)$$

and the time-evolution superoperator according to Eq. (1),

$$\mathcal{U}_i(\Delta t) \hat{\rho}_{\text{tot}}(t) = e^{-i\hat{H}_{\text{tot}}\Delta t/\hbar} \hat{\rho}_{\text{tot}}(t) e^{i\hat{H}_{\text{tot}}\Delta t/\hbar}.$$

The former corresponds to the rotation about the x axis by the angle π with an impulsive pulse, while the latter is the idling without pulses. In this study, we only consider impulsive pulses to eliminate errors during pulse application and focus on the effects of the free evolution $\mathcal{U}_i(\Delta t)$. The operator $\hat{R}_\alpha(\theta) = \exp[-i\theta\hat{\sigma}_\alpha/2]$ in Eq. (2) is the rotation operator about an α axis by an angle θ and is applied to the single-qubit subsystem. Note that the rotation operator $\hat{R}_x(\pi)$ in Eq. (2) is modified

to $\hat{R}_z(\omega_{\text{ext}}t)\hat{R}_x(\pi)\hat{R}_z(-\omega_{\text{ext}}t)$ [16] when one considers application of a continuous microwave with the frequency ω_{ex} to a transmon qubit [44]. Since most of the DD schemes are devised without this additional phase, we must pay attention when we consider the theories and experiments [45].

Since the system Hamiltonian and the system part of the interaction commute, $[\hat{H}_S, \hat{V}] = 0$, the dynamics of the system for the Ramsey, HE, and DD experiments are expressed in an analytical form. See Sec. III and Appendix A for more details.

Now, we specify a form of the spectral density to conduct simulations. The spectral density is given by

$$J_s(\omega) = \text{sgn}(\omega) \frac{\kappa \omega_{\text{ph}}^{1-s} |\omega|^s}{(1 + (\omega/\omega_c)^2)^2},$$

where ω_c and κ are the cutoff frequency and the coupling strength between the system and reservoir, respectively. The spectral exponent s determines the behavior of $J_s(\omega)$, and the quantity ω_{ph} has been introduced to fix the unit of κ irrespective of s .

Depending on the spectral exponent s , the spectral density is classified into the following three types: Ohmic ($s = 1$), super-Ohmic ($s > 1$), and sub-Ohmic ($0 < s < 1$) types. The spectral noise power for the Ohmic bath $S_{\beta, s=1}(\omega)$ corresponds to the white noise in the low frequency region, $S_{\beta, s=1}(\omega = 0) = \kappa k_B T$, while the sub-Ohmic baths represent $1/f^\epsilon$ noise, $S_{\beta, s < 1}(\omega \rightarrow 0) \simeq \kappa k_B T (\omega_{\text{ph}}/\omega)^{1-s}$. In the context of the transmon qubit, fluctuations of electromagnetic fields are modeled as an Ohmic reservoir [9, 46, 47], and $1/f^\epsilon$ noise is found [17, 48] as a result of two-level fluctuators [9, 49–51] and quasiparticles' dynamics [43]. On the basis of the above, we choose the values 1, 1/2, 1/4, 1/8, and 1/14 for the exponent s in this study. Further, we set ω_q as the unit of the frequency, and the other parameter values for the reservoir are set to $\beta \hbar \omega_q = 5$, $\omega_c = 50\omega_q$, $\omega_{\text{ph}} = \omega_q$, and $2\pi \hbar \kappa = 0.04$. Provided that the reservoir temperature is given by $T = 30\text{mK}$, the above parameter values indicate $\omega_q \simeq 2\pi \times 3.1\text{GHz}$.

For the numerical simulations, it is convenient to expand the autocorrelation function of the reservoir in a mathematically consistent way as follows:

$$C(t) = \sum_{k=1}^K d_k e^{-i\omega_k t - \gamma_k t} \quad (t > 0), \quad (3)$$

which was introduced to the free-pole hierarchical equations of motion (FP-HEOM) method [52]. To obtain the sets $\{d_k\}$, $\{\omega_k\}$, and $\{\gamma_k\}$ efficiently for a given accuracy, the barycentric representation of the spectral noise power $S_\beta(\omega)$ is exploited.

III. NUMERICAL RESULTS

In this section, we present results of the Ramsey experiments and investigate whether and to which extent

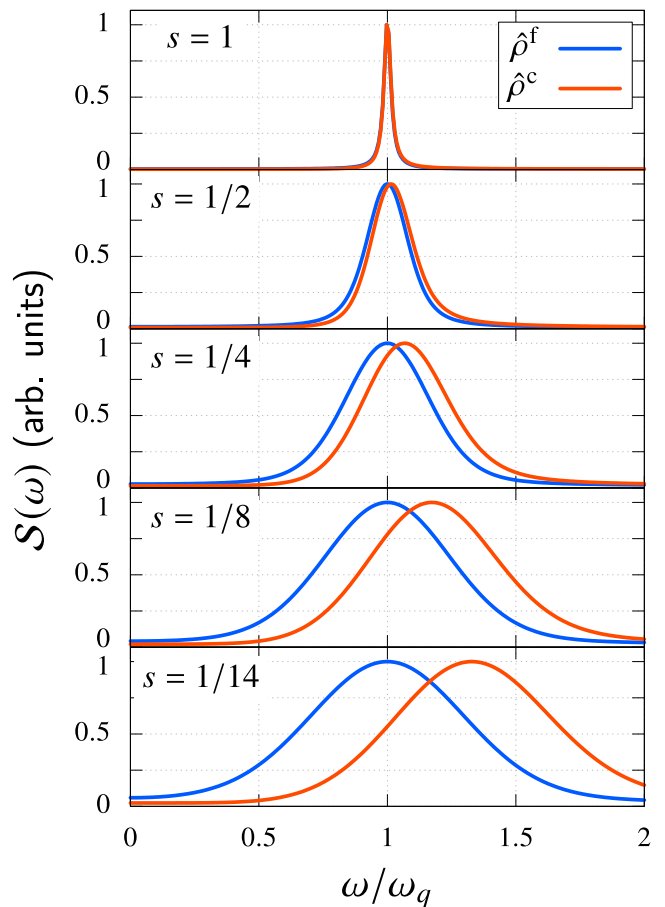


FIG. 1. Fourier transform of $\langle \hat{\sigma}_x(t) \rangle$ obtained with the Ramsey experiments, $S(\omega)$, with arbitrary (arb.) units. Each curve is normalized such that the maximum value is 1. The results with the factorized ($\hat{\rho}^f$, blue curve) and correlated ($\hat{\rho}^c$, red curve) initial state are depicted.

HE and DD improve the coherence time.

A. Ramsey experiments

Here, we discuss the results of the Ramsey experiments. Before the analysis of the numerical results, we make a brief remark on the different types of the initial state: We consider a factorized and correlated initial state in this study. The factorized initial state is defined as

$$\begin{aligned} \hat{\rho}_{\text{tot}}^f(0) &= \hat{R}_y\left(-\frac{\pi}{2}\right) |0\rangle\langle 0| \hat{R}_y\left(\frac{\pi}{2}\right) \otimes \hat{\rho}_{R,\text{eq}} \\ &= \frac{(|0\rangle + |1\rangle)(\langle 0| + \langle 1|)}{2} \otimes \hat{\rho}_{R,\text{eq}}, \end{aligned}$$

and the correlated one as

$$\hat{\rho}_{\text{tot}}^c(0) = \hat{R}_y\left(-\frac{\pi}{2}\right) \frac{e^{-\beta \hat{H}_{\text{tot}}}}{\text{tr}\{e^{-\beta \hat{H}_{\text{tot}}}\}} \hat{R}_y\left(\frac{\pi}{2}\right). \quad (4)$$

Here, the state $|0\rangle$ is the ground state of the qubit system (correspondingly, $|1\rangle$ indicates the first-excited state). In the latter preparation, all correlations caused by the total equilibrium state $e^{-\beta\hat{H}_{\text{tot}}}$ are taken into account. The former initial state is based on the assumption that during the preparation of the system into the ground state $|0\rangle\langle 0|$, equilibrium correlations caused by $e^{-\beta\hat{H}_{\text{tot}}}$ are destroyed.

Now, we start to discuss our results. In Fig 1, we depict the Fourier transform of $\langle\hat{\sigma}_x(t)\rangle = \text{tr}\{\hat{\sigma}_x\mathcal{U}_i(t)\hat{\rho}_{\text{tot}}(0)\}$,

$$\mathcal{S}(\omega) = \text{Re}\left\{\int_0^\infty dt \frac{\langle\hat{\sigma}_x(t)\rangle}{2} e^{-i\omega t}\right\},$$

where $\hat{\rho}_{\text{tot}}(0) = \hat{\rho}_{\text{tot}}^f(0)$ (the blue curve) and $\hat{\rho}_{\text{tot}}^c(0)$ (the red curve). There, one finds that the width of the profile is broader for the smaller spectral exponent s . The peak of $\mathcal{S}(\omega)$ for the factorized initial state is strictly at the value ω_q , while in the case with the correlated initial state, the peak is shifted to a larger frequency. In the following, we analyze these properties through the analytical expression of the reduced density operator (RDO) of the system.

Defining the off-diagonal element of the system RDO as $\rho_{eg}(t) = \langle 1|\hat{\rho}_S(t)|0\rangle = \langle 1|\text{tr}_R\{\hat{\rho}_{\text{tot}}(t)\}|0\rangle$, we evaluate the expectation value $\langle\hat{\sigma}_x(t)\rangle$ through the equation $\langle\hat{\sigma}_x(t)\rangle = 2\text{Re}\{\rho_{eg}(t)\}$. Here, $\text{tr}_R\{\bullet\}$ indicates the partial trace over the reservoir degrees of freedom. The dynamics of the off-diagonal element are derived as follows: for the factorized initial state,

$$\rho_{eg}(t) = \frac{1}{2} \exp\left[-i\omega_q t - 4 \int_0^t dt' \int_0^{t'} dt'' C'(t' - t'')\right] \quad (5)$$

and for the correlated initial state,

$$\rho_{eg}(t) = \rho_+(t) - \rho_-(t), \quad (6)$$

where the contribution of the ground and excited states, $\rho_+(t)$ and $\rho_-(t)$, are given by

$$\rho_\pm(t) = \frac{e^{\pm\beta\hbar\omega_q/2}}{2Z} \exp\left[-i\omega_q t \mp 4i \int_0^t dt' \bar{L}(t') - 4 \int_0^t dt' \int_0^{t'} dt'' C'(t' - t'')\right]. \quad (7)$$

Note that the function $\bar{L}(t) = -\int_t^\infty dt' C''(t')$ is proportional to the relaxation function of the reservoir [53]. Here, the real and imaginary part of the autocorrelation function are expressed through the relation $C(t) = C'(t) + iC''(t)$. The quantity Z is the partition function of the bare system, which is described as $Z = \text{tr}\{e^{-\beta\hat{H}_S}\} = 2 \cosh(\beta\hbar\omega_q/2)$.

First, we investigate the width of the profile. The term $\int dt' \int dt'' C'(t' - t'')$ in Eqs. (5) and (7) contributes to

the dynamics as decoherence, and we found that this integral is larger for smaller s in our study. This results in the broader peak for the smaller spectral exponent. Within the Born–Markov approximation, in the Ohmic and super-Ohmic cases, the decay rate caused by decoherence, $1/T_R$, is proportional to $S_\beta(0)$ (see Appendix A and Refs. 9 and 54). In the sub-Ohmic case, however, the spectral noise power diverges at $\omega = 0$, and this simple argument stemming from a perturbative treatment cannot be applied. In fact, the stronger divergence of $S_\beta(\omega)$ around $\omega \rightarrow 0$ for smaller exponents directly correlates with the tendency of T_R (cf. Table I for the time constant with the factorized initial state). Note that the width is the same for both factorized and correlated initial state.

Next, we focus on the frequency shift. For the factorized initial state, the reservoir does not change the Larmor frequency, as indicated by Eq. (5), and the peak of each blue curve is found at $\omega = \omega_q$ in Fig. 1. By contrast, the effective Larmor frequency is modified with the term $i \int dt' \bar{L}(t')$ in Eq. (7) in the case with the correlated initial state. Because we consider the low temperature $\beta\hbar\omega_q = 5$, the contribution of $\rho_-(t)$ to $\rho_{eg}(t)$ in Eq. (6) is small. The frequency of $\rho_+(t)$ at the time t is given by $\omega_q + 4 \int_0^t dt' \bar{L}(t')$ in Eq. (7), and we found that the function $\bar{L}(t)$ always takes nonnegative value in our simulations. For this reason, the peak for the correlated initial state is shifted to a larger frequency, which is indicated by the red curves in Fig. 1. The function $\bar{L}(t)$ decays slower as the spectral exponent s decreases, and hence the integral of $\bar{L}(t)$ takes larger values. This results in the larger shift of the red curve in Fig. 1 for the smaller exponent.

Note that the Lamb shift found in the conventional Born–Markov approximation approach [54–56] is independent of the above frequency shift: The Lamb shift results from correlations of the system and reservoir in the real-time domain, while the above frequency results from correlations between the total equilibrium state ($e^{-\beta\hat{H}_{\text{tot}}}$) and the real-time evolution $[\mathcal{U}_i(t)]$.

In the following numerical experiments, we evaluate the absolute value of the off-diagonal element $|\rho_{eg}(t)|$ to explore the impact of decoherence (dephasing). Due to the negligible contribution of $\rho_-(t)$, the absolute value is well approximated as $|\rho_{eg}(t)| \simeq |\rho_+(t)|$ at the low temperature. Since it turns out that for the given set of parameters differences in the normalized dynamics $|\rho_{eg}(t)|/|\rho_{eg}(0)|$ between the factorized and correlated initial states are negligibly small, we only discuss the former case in detail in the following study.

B. Hahn echo (HE)

In this section, we discuss the numerical results of the HE. The sequence of the HE is given by

$$\mathcal{U}_i(\Delta t') \mathcal{R}_x \mathcal{U}_i(\Delta t), \quad (8)$$

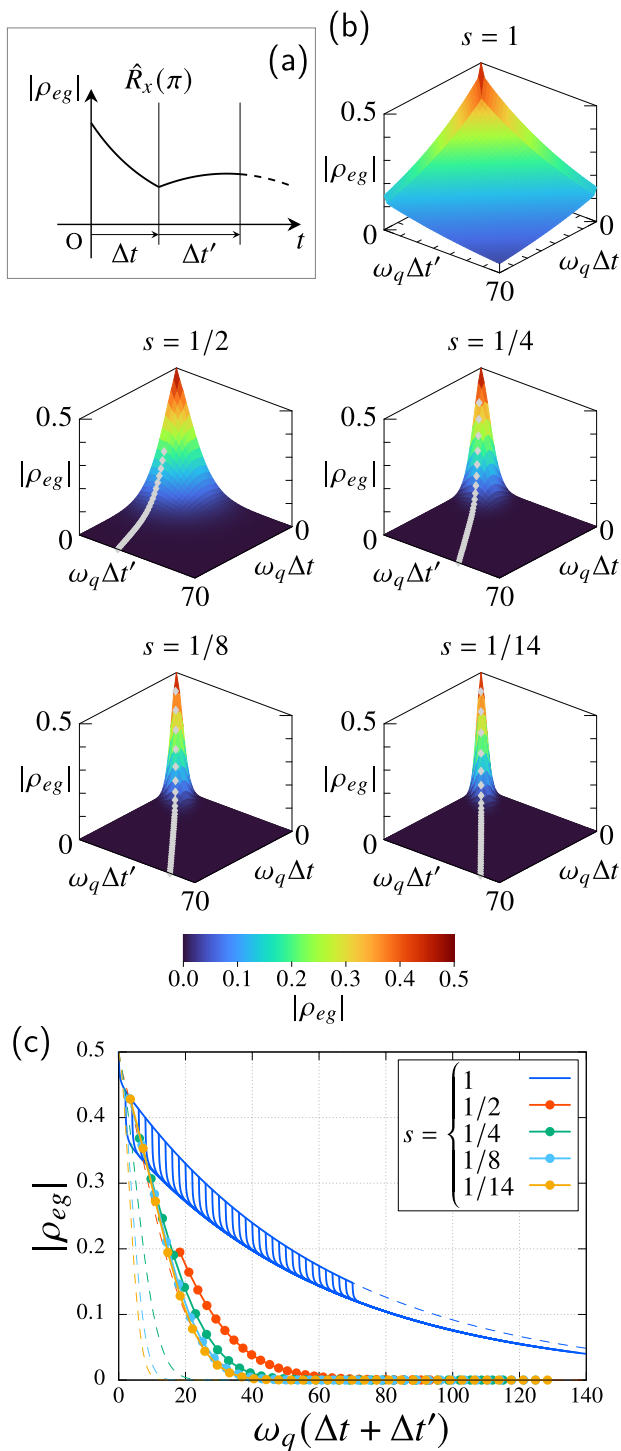


FIG. 2. (a) Schematic of the Echo experiment. (b) Dynamics of the off-diagonal element $|\rho_{eg}(t)|$ during the echo experiments. The gray diamonds indicate a local maximum of $|\rho_{eg}(t)|$ with respect to $\Delta t'$ with a fixed Δt . (c) Dynamics of the peak position and the whole dynamics of $|\rho_{eg}(t)|$ during the echo experiments. The filled circles correspond to the gray diamonds in (b). In the case for $s = 1$, the whole dynamics of $|\rho_{eg}(t)|$ are depicted instead of the peak position. The dashed curves are the dynamics without the pulse (Ramsey experiments).

TABLE I. Time constants of the decay of the off-diagonal element $|\rho_{eg}(t)|$ obtained from the Ramsey and echo experiments. The quantity T_R is the time constant of the Ramsey experiments, and T_E is the time constant of the echo experiments.

s	1	1/2	1/4	1/8	1/14
$\omega_q T_R$	62.5	16.9	7.82	5.39	4.46
$\omega_q T_E$	62.5	27.7	19.6	17.2	16.5

and the schematic of this sequence is displayed in Fig. 2(a). In the same way as the Ramsey experiment, the dynamics of $\rho_{eg}(t)$ is analytically evaluated. For details, see Appendix A.

Figure 2(b) displays the dynamics of the off-diagonal element of the RDO, $|\rho_{eg}(t_e)|$ starting at $|\rho_{eg}(t_e = 0)| = 1/2$. The time argument t_e is given by $t_e = \Delta t + \Delta t'$ [end of a single HE sequence, cf. Fig. 2(a)] with Δt and $\Delta t'$ being varied independently. Note that the curves along the line $\Delta t' = 0$ correspond to the Ramsey experiments without the $\hat{R}_x(\pi)$ pulse.

A general result of our simulations is that a recovery of $|\rho_{eg}(t)|$ is observed for sub-Ohmic reservoirs only, while the application of a pulse is always detrimental for Ohmic ones. In order to understand this, one has to recall that the echo technique was originally developed to reduce the effects of the “inhomogeneous broadening” in NMR experiments. This broadening results from the inhomogeneity of *static* magnetic fields which, within the framework of the system–reservoir model, corresponds to a time-independent two-time correlation function of the reservoir in the classical limit [57]. Now, for sub-Ohmic spectral densities the two-time correlator decays slower for smaller spectral exponents s which is to say that the reservoir tends to become gradually more sluggish. Accordingly, in the Ohmic case ($s = 1$), the relatively fast decay of the two-time correlation function is dominated by the large portion of higher-frequency modes in the region $\omega_q \ll \omega \lesssim \omega_c$, leading to the fast decay of $|\rho_{eg}(t)|$ in the HE experiments. With the growing portion of low-frequency modes in the spectral noise power, the strongly suppressed dynamics of the reservoir make it possible to mitigate the impact of decoherence by echo sequences. In order for this to be effective, the spectral exponent has to be lower than $s \approx 1/2$ since for this value the recovery is not yet observed in the short-time region $\omega_q \Delta t < 14$ [cf. Fig. 3(c) below with $s = 1/2$ in which a fast decay right after the pulse application is found, which corresponds to the dynamics of the echo experiment around the time $\Delta t' \simeq 0$].

To investigate to which extent the echo sequence improves the qubit’s coherence time, we depict in Fig. 2(c) the maximum recovered value of $|\rho_{eg}(t)|$: For a fixed Δt , we detect local maxima with respect to $\Delta t'$, and monitor the value of each local maximum as a function of the total time $\Delta t + \Delta t'$. These results are then compared with those of Ramsey experiments ($\Delta t' = 0$, cf. Sec. III A).

By way of example, in the Ohmic case ($s = 1$), the whole dynamics of $|\rho_{eg}(t)|$ are instead displayed for various values of Δt with the step-like decay corresponding to the pulse application. The time constants extracted from this analysis are listed in Table I, see also Appendix B. As already mentioned above, in the Ohmic case, the intensity significantly decreases right after the pulse application, where the overall decay time remains almost the same. By contrast, in the sub-Ohmic cases, the improvement of the time constant is more significant with an increasing ratio T_E/T_R for smaller spectral exponents. This implies that since the time-independent properties of the two-time correlation function are enhanced in the deep sub-Ohmic domain, the echo sequence works in a more efficient way. When the correlation function tends to be almost time-independent, the peak positions align along the diagonal in Fig. 2(b), again verifying that a deep sub-Ohmic reservoir behaves almost as a static reservoir on relevant timescales. Conversely, if we measure the signal with the condition $\Delta t = \Delta t'$, the time constants decrease compared to what is depicted in Fig. 2(c).

Note that while the improvement of the time constant from the Ramsey to the HE experiments is the most significant in the case $s = 1/14$, the absolute value of the time constant for the Ramsey experiment in this case is the smallest, as discussed in Sec. III A.

C. Dynamical decoupling (DD)

Next, we study the dynamics during DD experiments with the pulse sequence

$$\left\{ \mathcal{U}_i(\Delta t/2) \mathcal{R}_x \mathcal{U}_i(\Delta t) \mathcal{R}_x \mathcal{U}_i(\Delta t/2) \right\}^n \quad (9)$$

with integer $n > 1$. The schematic of this sequence is shown in Fig. 3(a). Here, we follow previous studies [25, 42, 58], and a symmetric version of the Carr–Purcell–Meiboom–Gill (CPMG) sequence is applied. Notably, while in previous studies [25, 42, 58, 59] only small to moderate durations Δt have been considered, here, we explore a wide range of idle durations from small values much below the qubit frequency to relatively large values beyond, i.e., $0.002 \leq \omega_q \Delta t \leq 10$. We again refer the readers to Appendix A for the analytical expression of the dynamics of $\rho_{eg}(t)$ during the sequence of Eq. (9).

By way of example, the dynamics with $\omega_q \Delta t = 4$ and $\omega_q \Delta t = 8$ for spectral exponents $s = 1, 1/2$, and $1/14$ are depicted in Fig. 3(c). Strikingly, one observes a different behavior for decreasing s when Δt grows: In the Ohmic regime a larger Δt implies improved coherences while the opposite is true in the deep sub-Ohmic regime. In order to explore this quantitatively, we extract from these time traces time constants T_{DD} for the decay of coherences in the presence of DD with varying Δt (for details see Appendix B) and depict them in Fig. 3(d). The total time of the time evolution for the evaluation of T_{DD} is fixed to $200/\omega_q$, so that we can obtain the total number

of pulses applied during the whole sequence accordingly (from 20 to 10^5).

In all cases, irrespective of the spectral exponent s , we can distinguish a domain for very short times $\omega_q \Delta t \ll 1$ with a steep drop of T_{DD} and a domain beyond with a much smoother behavior. In the latter domain the time constant T_{DD} increases and, deeper in the sub-Ohmic regime, approaches a local maximum before it tends to decrease again. The transition between these two time domains appears as a local minimum, the position of which shifts towards $\omega_q \Delta t \approx 1$ for decreasing spectral exponents.

In order to understand this behavior we first turn to the very-small- Δt region. There, one can consider the simplified pulse sequence of the HE, as discussed above, since the HE sequence also appears in the fundamental pulse sequence for the DD, cf. Eqs. (8) and (9). Results are shown in Fig. 3(b) for $\omega_q \Delta t = 0.1$. Apparently, in the very-short-time region after the application of a single Hahn-pulse a characteristic growth of coherences can be seen. In the short time regime $\omega_c \Delta t' \ll 1$, the fluctuation of \hat{V} caused by the reservoir can be seen as static, and thus the recovery of coherences is observed irrespective of the spectral exponent s . Right after this *universal recovery* of coherences, the system experiences decoherence when the duration of the first idle phase Δt is small. This decoherence is similar to the universal decoherence [10, 60]: Due to the relation $[\hat{H}_S, \hat{V}] = 0$, the decay of the coherence is determined only by the properties of the reservoir, whose representation is the same as the one for the universal decoherence (see Appendix A). The universal decoherence is slower for deeper sub-Ohmic reservoirs which in turn leads to larger timescales for the universal recovery. By contrast, when Δt increases, further recovery of coherence is observed for deep sub-Ohmic reservoirs, cf. inset of Fig. 3(b) for $\omega_q \Delta t = 1$ with $s = 1/14$: A fast increase of coherence in the region $1 \leq \omega_q(\Delta t + \Delta t') \leq 1.05$ is found and a subsequent slower increase, rather than universal decoherence, in the region $1.05 \leq \omega_q(\Delta t + \Delta t')$. We attribute the former steep increase to the universal behavior and the bending towards a slower increase to the recovery which is found in HE as well (we refer to this recovery as an HE-like recovery hereafter).

We conclude from this analysis that, if for a DD sequence, the next pulse is applied within this short time range, decoherence is indeed suppressed very efficiently. If the time between the first and the second pulse exceeds this time range, decoherence becomes substantial, very similar to what happens after application of a single HE.

Now, we turn to the analysis of the large- Δt region, $\omega_q \Delta t \geq 0.2$. In the Ohmic case, steep drops in $|\rho_{eg}(t)|$ are observed in Fig. 3(c). This is due to the relatively large portion of high-frequency modes in $S_\beta(\omega)$ as discussed above for the HE experiments. Larger values of Δt lead to decreasing relevance of these modes and, consequently, the decay of coherence slows down as Δt increases [left

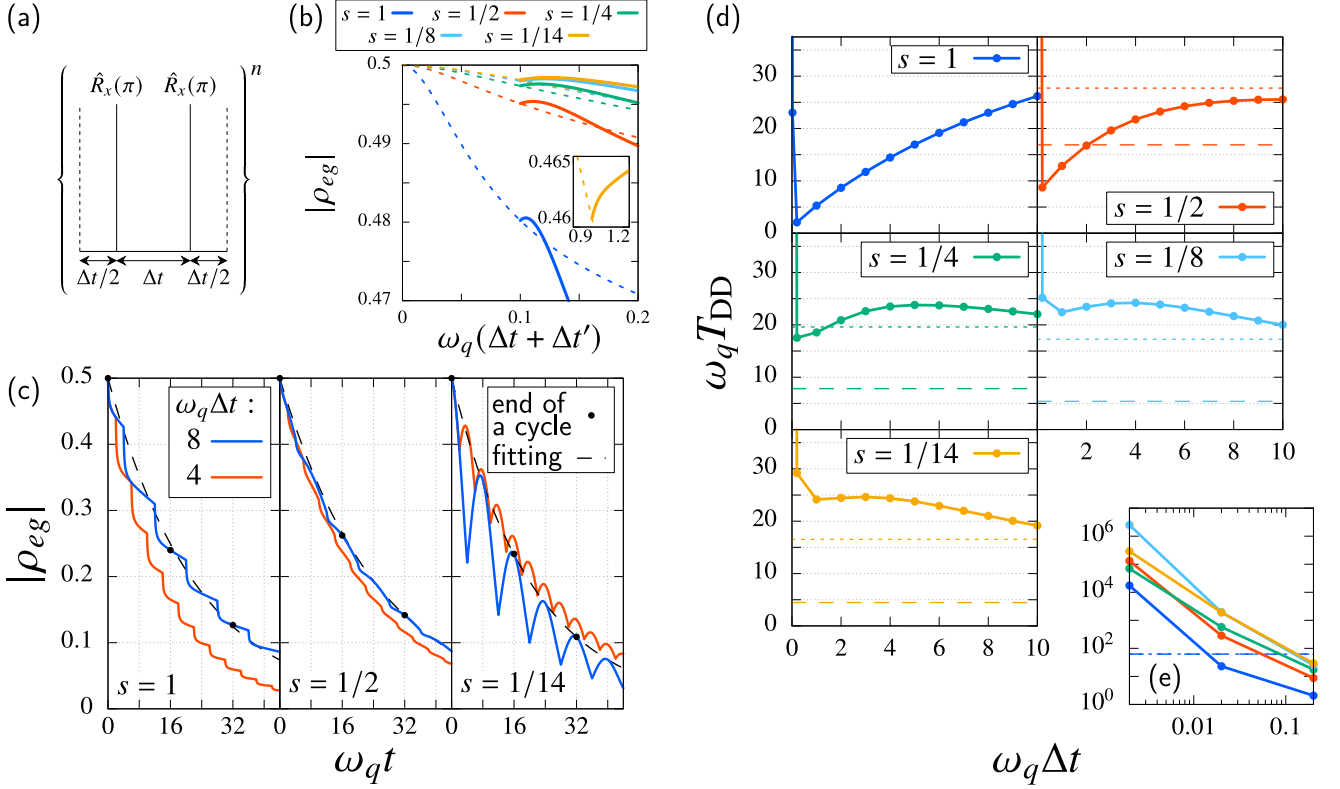


FIG. 3. (a) Schematic of the CPMG sequence. (b) Dynamics of $|\rho_{eg}(t)|$ during the Hahn-echo experiments in the short-time region. The duration is given by $\omega_q\Delta t = 0.1$. The dashed curve indicates the dynamics of the Ramsey experiments. In the inset, the same dynamics but with $\omega_q\Delta t = 1$ and $s = 1/14$ are plotted. (c) Dynamics of the off-diagonal element $|\rho_{eg}(t)|$ during the dynamical-decoupling experiments. As representatives, the cases $\omega_q\Delta t = 4$ and 8 for the spectral exponent $s = 1, 1/2$, and $1/14$ are depicted. The filled circles indicate the end of each cycle in the case $\omega_q\Delta t = 8$, and the dashed curves are fitted exponential functions obtained from the values of the filled circles. (d) Time constant of the decay T_{DD} with respect to the duration of the idle phase Δt . In the sub-Ohmic case, the time constants for the Ramsey and echo experiments, T_R and T_E , which are listed in Table I, are also depicted as the dashed and dotted line, respectively. (e) Log-log plot of T_{DD} in the small- Δt region. The time constants, T_R and T_E , in the Ohmic case are depicted here as the dashed and dotted blue line, respectively.

panel of Fig. 3(c), $s = 1$]; it even reverts to an increasing time constant T_{DD} in the region $\omega_q\Delta t \geq 0.2$.

In the deep sub-Ohmic domain, the steep drops discussed above are no longer observed. Instead, the HE-like recovery of the intensity is observed in Fig. 3(c) leading to an improved coherence time even beyond what can be achieved with HE and what is observed in a Ramsey experiment (no pulses). Here, the strong presence of low-frequency modes induces a smoother transition from the short to the moderate and the long time range. At $\omega_q\Delta t \approx 1$, the transition from the universal suppression of decoherence to the HE-like recovery appears. With increasing duration Δt beyond the local minimum in T_{DD} , decoherence between two successive pulses plays a significant role [right panel of Fig. 3(c)], and the time constant decreases. For example, in the case $s = 1/14$, this results even in a local maximum at $\omega_q\Delta t = 3$. The same discussion holds for the case $s = 1/8$.

The cases with $s = 1/2$ and $1/4$ are intermediate between those with $s = 1$ and $1/14$: In Fig. 3(c) with $s = 1/2$, the red curve displays the steep drop, although

the magnitude of this decay is smaller in comparison to the case $s = 1$. By contrast, the blue curve exhibits slight recoveries of the intensity in the middle and at the end of each cycle. This indicates that in the small- Δt region, $0.2 \leq \omega_q\Delta t \lesssim 4$, an improvement related to the fast decay is observed while in the longer Δt region, $\omega_q\Delta t \gtrsim 5$, the HE-like recovery appears.

We thus draw the following conclusions: (i) The time constant T_{DD} strongly depends on the duration Δt and the spectral exponent s . We would like to emphasize that the performance depends on the detailed profile of the spectral noise power: The comparison between ω_c and Δt , which has been conducted in previous studies [61] might be insufficient in some cases. (ii) For Ohmic reservoirs, the DD-approach never improves the time constant compared to HE and Ramsey experiments, unless for extremely short times $\omega_c\Delta t < 1$ with $\omega_q \ll \omega_c$. This corresponds to the “decoherence acceleration” found also in previous studies [25, 58]. (iii) For sub-Ohmic spectral densities with $1/4 < s \leq 1$ the application of DD is beneficial compared to Ramsey experiments but the time

constant still remains below the one seen in HE except for very short times. (iv) In the relatively deep sub-Ohmic range $s \leq 1/4$, the DD provides an improvement of the stability of coherence beyond both the HE and Ramsey findings for almost all parameter values; a few exceptions are found in our results for $\omega_q \Delta t = 0.2$ and 1 with $s = 1/4$.

Now, we comment on predictions in previous studies. The prediction of the decrease in the coherence time T_{DD} in the very-short-time region $\omega_c \Delta t < 1$ in previous studies [62, 63] is consistent with our results. In previous experiments [19, 34], local maxima of T_{DD} were found, which was attributed to imperfect pulses. Our results suggest that local maxima is observed even with perfect pulses, for timescales sufficiently larger than those of the cutoff frequency of the reservoir.

As a final technical remark we mention that our simulations provide somewhat less accurate results in the very-short-time region $\omega_q \Delta t \leq 0.02$. As illustrated in Fig. 3(e), the decay is very slow in the region $\omega_q \Delta t \leq 0.02$ (orders of magnitudes larger T_{DD} than that for longer Δt) so that numerical calculations are extremely susceptible to even tiny numerical errors. We observed, however, that the degrading accuracy of the results does not change the qualitative profile in Fig. 3(e), that is, the decrease of T_{DD} up to the duration $\omega_q \Delta t = 0.2$ as well as the acceleration of decoherence for $\omega_q \Delta t \geq 0.02$ in the Ohmic case.

IV. CONCLUDING REMARKS

In this contribution, we numerically studied pure-dephasing dynamics of a single qubit, focusing on effects of the static qubit–reservoir correlation at an initial time and the performance of typical quantum control techniques, such as Hahn echo (HE) and dynamical decoupling (DD). For further understanding of the qubit’s dynamics and the applicability of those control techniques, we chose specific spectral densities relevant for superconducting quantum devices. The class of the spectral densities considered in this study covers from typical Ohmic noise, which corresponds to the white noise in a certain limit, to deep sub-Ohmic noise, which represents $1/f^\epsilon$ -type noise in small-frequency region. For the DD simulations, we studied the whole dynamics of a single qubit in time with a wide range of the time interval between two pulses (duration of the idle phase). This contrasts with a lot of previous studies, which focused on stroboscopic behavior at the end of a sequence in the small interval limit $\Delta t \rightarrow 0$.

For the Ramsey experiments, the shift of the effective Larmor frequency caused by the correlated equilibrium state $e^{-\beta \hat{H}_{\text{tot}}}$ was found. The deviation from the frequency of the bare system ω_q depends on the profile of the spectral density: The slow decay of the two-time correlation function, i.e. the large portion of the low-frequency modes of the spectral density, contributes the frequency

shift. It is worth noting that not only the Lamb shift, which originates from the correlation between the system and bath during the real-time evolution, but also the initial correlation affect the effective Larmor frequency.

For the HE sequences, the improvement of the coherence time was quantitatively analyzed. Exploring the whole dynamics during the HE sequence, we found that the recovery of the coherence $|\rho_{eg}(t)|$ occurs in the sub-Ohmic case ($s \leq 1/2$), while the echo pulse always deteriorates the coherence in the Ohmic case ($s = 1$). As theoretically predicted, the improvement is most significant for the deepest sub-Ohmic bath ($s = 1/14$), which generates the *nearly static* noise.

In the DD simulation, the performance of the CPMG sequence was investigated. As expected, we found that when the timescale of the pulse interval is sufficiently shorter than those for the reservoir cutoff frequencies ($\omega_c \Delta t \ll 1$), coherences are stabilized irrespective of the bath spectral density, which corresponds to previous studies [25, 61]. The main focus has been on the performance for longer pulse duration in agreement with the experimental situation: Interestingly, for sub-Ohmic baths coherence times are substantially enhanced compared to simple Ramsey results due to reservoir-induced feedback. For reservoirs with exponents $s < 1/2$, even local maxima of coherence times can be identified around pulse intervals on the order of the qubit transition frequency. By contrast, the coherence time for DD is worse than that for Ramsey experiments in the Ohmic case ($s = 1$) once the condition $\omega_c \Delta t \gg 1$ is violated. We conclude that neither HE nor DD can stabilize coherence in the pure Ohmic case. Overall, we have obtained a comprehensive picture of the DD performance depending on not only the time interval Δt but also the profile of the spectral noise power, especially the spectral exponent s . These results together with respective simulations employing the platform used here can now be adopted to actual experimental settings to optimize pulse forms but also to characterize noise.

In this study, the coupling form between the system and reservoir is restricted to the pure-dephasing type in order to focus on the profile of the noise spectral density affecting the decoherence dynamics and performance of the HE and DD scheme. The impulsive pulse with the zero width is also adopted for the same purpose. Studies of the noise effects on various DD schemes that can compensate for errors originating from the population relaxation of the system and accumulating during finite-width pulse application can be conducted along the same lines as in this study: For example, numerically rigorous simulations of dynamics of a single qubit during a sequence consisting of three pulses with a finite width interleaved with two idle phases have already been reported in a previous study [16]. The application of the method to these cases is left to future works.

ACKNOWLEDGEMENT

The authors would like to thank J. T. Stockburger for fruitful discussions. This work was supported by the BMBF through QSolid and the Cluster4Future QSens (Project QComp) and the DFG through Grant No. AN336/17-1 (FOR2724). Support by the state of Baden-Württemberg through bwHPC and the German Research Foundation (DFG) through Grant No. INST 40/575-1 FUGG (JUSTUS 2 cluster) is also acknowledged.

Appendix A: The path-integral representation of the RDO for pure-dephasing simulations

In this section, we derive an equation for the dynamics of the RDO controlled by the Hahn-echo and dynamical-decoupling schemes, which was discussed in Sec. III. In those simulations, we only considered the impulsive pulses, and therefore we only need to consider the time evolution of the idle phases. For those simulations, a quantum Gaussian environment is considered, leading to the Hamiltonian in the form of

$$\hat{H}_R = \sum_j \left(\frac{\hat{p}_j^2}{2m_j} + \frac{1}{2} m_j \omega_j^2 \hat{x}_j^2 \right), \quad \hat{X} = \sum_j c_j \hat{x}_j$$

in Eq. (1). Namely, the reservoir consists of an infinite number of harmonic oscillators, with \hat{p}_j , \hat{x}_j , m_j , and ω_j being the momentum, position, mass, and angular frequency of the j th bath, respectively. The coupling strength between the system and j th oscillator, c_j , defines the spectral density as

$$J(\omega) = \sum_j \frac{c_j^2}{2m_j\omega_j} \delta(\omega - \omega_j).$$

When we introduce the eigenvectors of the system Hamiltonian, $\hat{\sigma}_z |a\rangle = (-1)^{a+1} |a\rangle$ ($a = 0, 1$), and the eigenvectors of the position operator of the reservoir, $|\mathbf{x}\rangle = |x_1, \dots, x_j, \dots\rangle$, the time-evolution operator for the total Hamiltonian in Eq. (1) is evaluated as

$$\begin{aligned} & \langle b, \mathbf{x}' | e^{-i\hat{H}_{\text{tot}}t/\hbar} | a, \mathbf{x} \rangle \\ &= \delta_{ab} e^{-i\omega_a t} \left\langle \mathbf{x}' \left| \exp \left[-\frac{i}{\hbar} \left(\hat{H}_R - (-1)^{a+1} \hbar \hat{X} \right) t \right] \right| \mathbf{x} \right\rangle, \end{aligned}$$

where δ_{ab} is the Kronecker delta and $\omega_a = (-1)^{a+1} \omega_q/2$. The Boltzmann distribution $e^{-\beta\hat{H}_{\text{tot}}}$ is also evaluated in the same way with the replacement of it/\hbar with β . Note that the system part of the total Hamiltonian is replaced with c -numbers, and the bracket only includes the reservoir operators. Considering the time evolution, $e^{-i\hat{H}_{\text{tot}}t/\hbar} \hat{\rho}_{\text{tot}}^c(0) e^{i\hat{H}_{\text{tot}}t/\hbar}$, where $\hat{\rho}_{\text{tot}}^c(0)$ is given by Eq. (4), we obtain the matrix element of the RDO $\rho_{ab}(t) = \langle a | \hat{\rho}_S(t) | b \rangle$ in the following form by tracing out

the reservoir degrees of freedom:

$$\begin{aligned} & \rho_{ab}(t) \\ &= e^{-i\omega_{ab}t} \sum_c \left\langle a \left| \hat{R}_y \left(-\frac{\pi}{2} \right) \right| c \right\rangle \frac{e^{-\beta\hbar\omega_c}}{Z} \left\langle c \left| \hat{R}_y \left(\frac{\pi}{2} \right) \right| b \right\rangle \\ & \times \exp \left[-\int_0^t dt' \int_0^{t'} dt'' v_{ab}^2 C'(t' - t'') \right. \\ & \quad \left. + i \int_0^t dt' \int_0^{\beta\hbar} d\tau' v_{ab} \bar{C}(-t' - i\tau') (-1)^{c+1} \right], \end{aligned} \quad (\text{A1})$$

where $\omega_{ab} = \omega_a - \omega_b$ is the difference of the frequency between the bra- and ket-vectors, and $Z = \text{tr}\{e^{-\beta\hat{H}_S}\} = 2 \cosh(\beta\hbar\omega_q/2)$ is the partition function of the bare system. Note that the first term of the exponent corresponds to the conventional influence functional introduced in the Feynman-Vernon path integral representation [64], and $v_{ab} = (-1)^{a+1} - (-1)^{b+1}$ corresponds to the commutator $[\hat{V}, \bullet]$. The contribution of the imaginary part of the two-time correlation function $C''(t)$ is always zero in our study.

The second term of the exponent originates from the correlated initial state and describes correlations between the Boltzmann distribution of the total Hamiltonian $e^{-\beta\hat{H}_{\text{tot}}}$ and the time-evolution operator $e^{\pm i\hat{H}_{\text{tot}}t/\hbar}$. The extended two-time correlation function is defined as

$$\bar{C}(z) = \hbar \int_0^\infty d\omega J(\omega) \frac{\cosh\left(\frac{\beta\hbar\omega}{2} - i\omega z\right)}{\sinh\left(\frac{\beta\hbar\omega}{2}\right)}.$$

If the variable z is a real number, $z \in \mathbb{R}$, the function $\bar{C}(z)$ coincides with $C(t)$.

Note that the influence functional with the correlated initial state includes the term

$$\exp \left[\int_0^{\beta\hbar} d\tau' \int_0^{\tau'} d\tau'' \bar{C}(-i\tau' + i\tau'') \right] = e^{-\beta\lambda}, \quad (\text{A2})$$

which is derived under the condition $[\hat{H}_S, \hat{V}] = 0$. The quantity $\lambda = \hbar^2 \int_0^\infty d\omega J(\omega)/\omega$ is the reorganization energy. This term only shifts the origin of the energy and is omitted with the normalization condition at $t = 0$.

For the Hahn-echo experiment, the pulse sequence in the superoperator representation is given by Eq. (8), and corresponding time evolution is evaluated as

$$\begin{aligned} & \langle b, \mathbf{x}' | e^{-i\hat{H}_{\text{tot}}\Delta t'/\hbar} \hat{R}_x(\pi) e^{-i\hat{H}_{\text{tot}}\Delta t/\hbar} | a, \mathbf{x} \rangle \\ &= e^{-i(\omega_b\Delta t' + \omega_a\Delta t)} \langle b | \hat{R}_x(\pi) | a \rangle \\ & \times \left\langle \mathbf{x}' \left| \exp \left[-\frac{i}{\hbar} \left(\hat{H}_R - (-1)^{b+1} \hbar \hat{X} \right) \Delta t' \right] \right. \right. \\ & \quad \left. \left. \times \exp \left[-\frac{i}{\hbar} \left(\hat{H}_R - (-1)^{a+1} \hbar \hat{X} \right) \Delta t \right] \right| \mathbf{x} \right\rangle. \end{aligned}$$

By using this relation, the matrix element of the RDO at the time $t_e = \Delta t' + \Delta t$ is derived as

$$\begin{aligned} & \rho_{ab}(t_e) \\ &= \sum_{c,d,e} e^{-i(\omega_{ab}\Delta t' + \omega_{de}\Delta t)} \langle a | \hat{R}_x(\pi) | d \rangle \langle e | \hat{R}_x(-\pi) | b \rangle \\ & \quad \times \left\langle d \left| \hat{R}_y\left(-\frac{\pi}{2}\right) \right| c \right\rangle \frac{e^{-\beta\hbar\omega_c}}{Z} \left\langle c \left| \hat{R}_y\left(\frac{\pi}{2}\right) \right| e \right\rangle F(t_e), \end{aligned} \quad (\text{A3})$$

where

$$\begin{aligned} F(t_e) = \exp & \left[- \int_0^{t_e} dt' \int_0^{t'} dt'' v^\times(t') C'(t' - t'') v^\times(t'') \right. \\ & \left. + i \int_0^{t_e} dt' \int_0^{t'} dt'' v^\times(t') \bar{C}'(-t' - i\tau'') (-1)^{c+1} \right]. \end{aligned} \quad (\text{A4})$$

Here, $v^\times(t) = v(t) - v'(t)$ is the commutator, and we have defined $v(t)$ and $v'(t)$ as

$$\begin{aligned} v(t) &= \begin{cases} (-1)^{d+1} & (0 \leq t \leq \Delta t) \\ (-1)^{a+1} & (\Delta t \leq t \leq \Delta t + \Delta t') \end{cases}, \\ v'(t) &= \begin{cases} (-1)^{e+1} & (0 \leq t \leq \Delta t) \\ (-1)^{b+1} & (\Delta t \leq t \leq \Delta t + \Delta t') \end{cases}. \end{aligned}$$

Again, the imaginary part $C''(t)$ does not contribute to the dynamics.

For the dynamical-decoupling simulations, the time-evolution operator corresponding to Eq. (9) is expressed as

$$\begin{aligned} & e^{-i\hat{H}_{\text{tot}}t_{2n+1}/\hbar} \hat{R}_x(\pi) e^{-i\hat{H}_{\text{tot}}t_{2n}/\hbar} \hat{R}_x(\pi) \\ & \quad \times \cdots \times \hat{R}_x(\pi) e^{-i\hat{H}_{\text{tot}}t_2/\hbar} \hat{R}_x(\pi) e^{-i\hat{H}_{\text{tot}}t_1/\hbar}, \end{aligned}$$

where $t_1 = \Delta t/2$ and $t_2 = t_3 = \cdots = t_{2n} = \Delta t$. At the end of the CPMG sequence, the value t_{2n+1} is given by $\Delta t/2$, while we vary t_{2n+1} to numerically obtain the whole dynamics. The matrix element of the RDO $\rho_{a_{2n+1}b_{2n+1}}(t_e)$ at the time $t_e = \sum_{l=1}^{2n+1} t_l$ is described as

$$\begin{aligned} & \hat{\rho}_{a_{2n+1}b_{2n+1}}(t_e) \\ &= e^{-i\omega_{a_{2n+1}b_{2n+1}}t_{2n+1}} \sum_{\substack{a_1, \dots, a_{2n} \\ b_1, \dots, b_{2n}}} F(t_e) \\ & \quad \times \sum_c \left\langle a_1 \left| \hat{R}_y\left(-\frac{\pi}{2}\right) \right| c \right\rangle \frac{e^{-\beta\hbar\omega_c}}{Z} \left\langle c \left| \hat{R}_y\left(\frac{\pi}{2}\right) \right| b_1 \right\rangle \\ & \quad \times \prod_{l=1}^{2n} e^{-i\omega_{a_l b_l} t_l} \langle a_{l+1} | \hat{R}_x(\pi) | a_l \rangle \langle b_l | \hat{R}_x(-\pi) | b_{l+1} \rangle. \end{aligned} \quad (\text{A5})$$

The function $F(t_e)$ takes the same form as Eq. (A4), but $v(t)$ and $v'(t)$ take different forms as follows:

$$\begin{aligned} v(t) &= (-1)^{a_l+1}, \\ v'(t) &= (-1)^{b_l+1}, \end{aligned}$$

which is defined for the interval $\tilde{t}_{l-1} \leq t \leq \tilde{t}_l$ ($l = 1, \dots, 2n+1$), where $\tilde{t}_0 = 0$ and $\tilde{t}_l = \sum_{j=1}^l t_j$ ($l \geq 1$). To evaluate the density operator with the factorized initial state, we replace the initial Boltzmann distribution in Eqs. (A1), (A3) and (A5) as $e^{-\beta\hbar\omega_0}/Z \rightarrow 1$ and $e^{-\beta\hbar\omega_1}/Z \rightarrow 0$ and set the term $(-1)^{c+1}$ in the influence functional to 0.

Here, we describe the concrete form of the off-diagonal element of the RDO with the factorized initial state, utilizing the relation $\rho_{eg}(t) = \rho_{10}(t)$. For the Ramsey experiment, in which no pulses are applied, it is derived as

$$\begin{aligned} & \rho_{eg}(t) \\ &= \frac{1}{2} e^{-i\omega_q t} \exp \left[-4 \int_0^t dt' \int_0^{t'} dt'' C'(t' - t'') \right] \\ &= \frac{1}{2} e^{-i\omega_q t} \exp \left[-4\hbar \int_0^\infty d\omega J(\omega) \coth \frac{\beta\hbar\omega}{2} \frac{1 - \cos \omega t}{\omega^2} \right]. \end{aligned} \quad (\text{A6})$$

For the echo experiment with $\Delta t' = \Delta t$, we obtain

$$\begin{aligned} & \rho_{eg}(t_e = 2\Delta t) \\ &= \frac{1}{2} \exp \left[-4\hbar \int_0^\infty d\omega J(\omega) \coth \frac{\beta\hbar\omega}{2} \right. \\ & \quad \left. \times \frac{1 - \cos 2\omega\Delta t}{\omega^2} \tan^2 \frac{\omega\Delta t}{2} \right], \end{aligned} \quad (\text{A7})$$

and for the dynamical decoupling with $t_{2n+1} = 0$ and $t_1 = \Delta t$ (an asymmetric version of the CPMG sequence), we obtain

$$\begin{aligned} & \rho_{eg}(t_e = 2n\Delta t) \\ &= \frac{1}{2} \exp \left[-4\hbar \int_0^\infty d\omega J(\omega) \coth \frac{\beta\hbar\omega}{2} \right. \\ & \quad \left. \times \frac{1 - \cos 2n\omega\Delta t}{\omega^2} \tan^2 \frac{\omega\Delta t}{2} \right]. \end{aligned} \quad (\text{A8})$$

Note that Eqs. (A6)–(A8) correspond to equations in previous studies [25, 42, 48, 58]. It is worth noting that the form of Eq. (A6) corresponds to that for the universal decoherence of the diagonal element of the RDO [10, 16, 60].

Ramsey experiments with Markov approximation

By differentiating Eq. (A6), we obtain the equation of motion for the off-diagonal element of the RDO as follows:

$$\dot{\rho}_{eg}(t) = - \left[i\omega_q + 4 \int_0^t dt'' C'(t - t'') \right] \rho_{eg}(t).$$

If we impose the Markov approximation, in which the two-time correlation function is localized at the time $t \simeq 0$, we can change the lower limit of the integration from 0 to $-\infty$, and the equation reads

$$\dot{\rho}_{eg}(t) = -(i\omega_q + \gamma_{pd})\rho_{eg}(t).$$

The pure-dephasing rate γ_{pd} is expressed as

$$\gamma_{pd} = 4\pi \lim_{\omega \rightarrow 0} S_\beta(\omega) = 2\pi\hbar \lim_{\omega \rightarrow 0} J(\omega) \coth \frac{\beta\hbar\omega}{2},$$

which coincides with the rate obtained from the Lindblad equation [54] and noninteracting-blip approximation (NIBA) [9]. As discussed in the main text, the above value diverges in the sub-Ohmic case, and this argument cannot be applied.

Dynamical decoupling in small Δt limit

Due to the cutoff function, $J(\omega)$ fast decays to 0 in the region $\omega \geq \omega_c$. When we consider the condition $\omega_c\Delta t \ll 1$, which corresponds to the small Δt limit, the term $\tan^2(\omega\Delta t/2)$ in the integrand in Eq. (A8) is approximated with $(\omega\Delta t/2)^2$. If the number n is large enough, the term $\cos 2n\omega\Delta t$ exhibits fast oscillation with respect to ω , and its contribution to the integral becomes negligibly small. Consequently, the off-diagonal element at a long enough time is evaluated as

$$\begin{aligned} & \rho_{eg}(t_e = 2n\Delta t) \\ & \simeq \frac{1}{2} \exp \left[-\hbar\Delta t^2 \int_0^\infty d\omega J(\omega) \coth \frac{\beta\hbar\omega}{2} \right], \end{aligned} \quad (\text{A9})$$

which corresponds to the asymptotic saturation pointed out in a previous study [58]. We confirmed that the exponent of Eq. (A9) is smaller for the smaller spectral exponent s (deeper sub-Ohmic reservoirs) in our simulation. This indicates that the saturated value of $\rho_{eg}(t_e = 2n\Delta t \gg 1/\omega_q)$ is larger for the smaller s in the small Δt limit. Assuming that the function $\rho_{eg}(2n\Delta t)$ monotonically decays with respect to n , which is true in our study, we deduce that the time constant T_{DD} is larger when the spectral exponent s decreases. This prediction deviates from the numerical results in Fig. 3(e), which results from the numerical errors discussed in the main text. Note that Eq. (A9) is derived on the basis of an asymmetric version of the CPMG sequence ($\Delta t_{2n+1} = 0$ and $t_1 = \Delta t$), while the sequence in the main text is a symmetric version ($\Delta t_{2n+1} = \Delta t_1 = \Delta t/2$).

Numerical implementation

To obtain numerical results, we evaluate the time derivatives, $\partial\rho_{eg}(t)/\partial t$ for Eq. (A1) and $\partial\rho_{eg}(t_e)/\partial t_e$ for Eqs. (A3) and (A5). For both factorized and correlated

initial states, we need to evaluate the function

$$\gamma'(t; \tau'', \tau') = \int_{\tau'}^{\tau''} dt'' C'(t - t''), \quad (\text{A10})$$

which appears in those time derivatives. Note that we can compute this function with the aid of the representation of the two-time correlation function in Eq. (3).

The function $\bar{L}(t)$ in Eq. (7) is the integral of $\bar{C}(-t' - i\tau')$ with respect to τ' and given by

$$\begin{aligned} \bar{L}(t) &= \hbar \int_0^\infty d\omega \frac{J(\omega)}{\omega} \cos \omega t \\ &= \frac{1}{2} \int_0^{\beta\hbar} d\tau' \bar{C}(-t - i\tau') = - \int_t^\infty dt' C''(t'). \end{aligned}$$

Note that the relaxation function of the reservoir $\Psi(t)$ is proportional to $\bar{L}(t)$, as $\Psi(t) = 2\bar{L}(t)/\hbar$ [53]. For the Hahn echo and dynamical decoupling, the off-diagonal element is given by $\rho_{eg}(t) = \rho_+(t) - \rho_-(t)$ with the following replacement in Eq. (7):

$$\begin{aligned} \omega_q t &\rightarrow \omega_q (\Delta t' - \Delta t) \quad (\text{Hahn echo}), \\ &\rightarrow \omega_q \sum_{l=1}^{2n+1} (-1)^{l+1} t_l \quad (\text{dynamical decoupling}), \\ 4 \int_0^t dt' \int_0^{t'} dt'' C(t' - t'') & \\ &\rightarrow \int_0^t dt' \int_0^{t'} dt'' v^\times(t') C(t' - t'') v^\times(t''), \\ 4i \int_0^t dt' \bar{L}(t') &\rightarrow 2i \int_0^t dt' v^\times(t') \bar{L}(t'). \end{aligned}$$

Similar to the evaluation of $\gamma'(t; \tau'', \tau')$ in Eq. (A10), the function $\bar{L}(t)$ is computed with the aid of Eq. (3): We solve the equation $d\bar{L}(t)/dt = C''(t)$ with the initial condition $\bar{L}(0) = \lambda/\hbar$ [λ is the reorganization energy in Eq. (A2)].

Appendix B: Time constants for the Ramsey, echo and dynamical-decoupling experiments

In this appendix we explain the fitting methods to obtain the time constants in Sec. III. We conducted the method of least squares and evaluated the time constants T_R , T_E and T_{DD} . In the Ramsey experiments for $s = 1$ and $1/2$, fast decay of $|\rho_{eg}(t)|$ was observed. Therefore, we considered the following functions as model curves;

$$|\bar{\rho}_{eg}(t)|_{(1)} = A \exp[-Bt] + C \exp[-Dt] + E, \quad (\text{B1})$$

$$|\bar{\rho}_{eg}(t)|_{(2)} = A \exp[-Bt] + C \exp[-(Dt)^2] + E, \quad (\text{B2})$$

and compared the residuals of the method of least squares. In the case for $s = 1$, a smaller residual was obtained with the curve for Eq. (B1) compared to the curve for Eq. (B2), while the opposite result was obtained in

the case $s = 1/2$. In both cases, T_R was evaluated with the relation $T_R = 1/D$. Here, we have defined $D < B$ in the Ohmic case, and the relation $D < B$ holds in the case $s = 1/2$.

In the other cases of the Ramsey experiments, the cases of the HE experiments with the condition $s \neq 1$, and all the cases of the DD experiments, fast decay was not observed, and we considered an exponential function,

$$|\bar{\rho}_{eg}(t)|_{(3)} = a \exp[-bt] + c,$$

and a Gaussian function,

$$|\bar{\rho}_{eg}(t)|_{(4)} = a \exp[-(bt)^2] + c$$

as model curves. In the Ramsey cases for $s \leq 1/4$ and the HE cases for $s \neq 1$, we found that the Gaussian fitting was better than the exponential fitting. For the DD experiments, we obtained better results with the exponential fitting compared to the Gaussian fitting.

For the HE experiment for $s = 1$, we evaluated the time constant from the asymptotic behavior of $|\rho_{eg}(t)|$: we found from Fig. 2(c) that the dynamics after the fast decay with different Δt can be represented by a single curve. We used this curve for the evaluation. The model curve $|\bar{\rho}_{eg}(t)|_{(3)}$ and $|\bar{\rho}_{eg}(t)|_{(4)}$ were considered, and the exponential fitting was found to be better. The time constants obtained with these curves are listed and plotted in Table I and Fig. 3(d), respectively.

-
- [1] A. P. M. Place, L. V. H. Rodgers, P. Mundada, B. M. Smitham, M. Fitzpatrick, Z. Leng, A. Premkumar, J. Bryon, A. Vrajitoarea, S. Sussman, *et al.*, New material platform for superconducting transmon qubits with coherence times exceeding 0.3 milliseconds, *Nat. Commun.* **12**, 1779 (2021).
- [2] C. Wang, X. Li, H. Xu, Z. Li, J. Wang, Z. Yang, Z. Mi, X. Liang, T. Su, C. Yang, *et al.*, Towards practical quantum computers: transmon qubit with a lifetime approaching 0.5 milliseconds, *npj Quantum Inf.* **8**, 3 (2022).
- [3] V. Negîrneac, H. Ali, N. Muthusubramanian, F. Battistel, R. Sagastizabal, M. S. Moreira, J. F. Marques, W. J. Vlothuizen, M. Beekman, C. Zachariadis, *et al.*, High-Fidelity Controlled-Z Gate with Maximal Intermediate Leakage Operating at the Speed Limit in a Superconducting Quantum Processor, *Phys. Rev. Lett.* **126**, 220502 (2021).
- [4] Y. Sung, L. Ding, J. Braumüller, A. Vepsäläinen, B. Kannan, M. Kjaergaard, A. Greene, G. O. Samach, C. McNally, D. Kim, *et al.*, Realization of High-Fidelity CZ and ZZ-Free iSWAP Gates with a Tunable Coupler, *Phys. Rev. X* **11**, 021058 (2021).
- [5] A. Kandala, K. X. Wei, S. Srinivasan, E. Magesan, S. Carnevale, G. A. Keefe, D. Klaus, O. Dial, and D. C. McKay, Demonstration of a High-Fidelity CNOT Gate for Fixed-Frequency Transmons with Engineered ZZ Suppression, *Phys. Rev. Lett.* **127**, 130501 (2021).
- [6] F. Arute, K. Arya, R. Babbush, D. Bacon, J. C. Bardin, R. Barends, R. Biswas, S. Boixo, F. G. S. L. Brandao, D. A. Buell, *et al.*, Quantum supremacy using a programmable superconducting processor, *Nature (London)* **574**, 505 (2019).
- [7] Google Quantum AI, Suppressing quantum errors by scaling a surface code logical qubit, *Nature (London)* **614**, 676 (2023).
- [8] Y. Kim, A. Eddins, S. Anand, K. X. Wei, E. van den Berg, S. Rosenblatt, H. Nayfeh, Y. Wu, M. Zaletel, K. Temme, *et al.*, Evidence for the utility of quantum computing before fault tolerance, *Nature (London)* **618**, 500 (2023).
- [9] U. Weiss, *Quantum Dissipative Systems*, 4th ed. (World Scientific, Singapore, 2012).
- [10] J. Tuorila, J. Stockburger, T. Ala-Nissila, J. Ankerhold, and M. Möttönen, System-environment correlations in qubit initialization and control, *Phys. Rev. Research* **1**, 013004 (2019).
- [11] A. P. Babu, J. Tuorila, and T. Ala-Nissila, State leakage during fast decay and control of a superconducting transmon qubit, *npj Quantum Inf.* **7**, 30 (2021).
- [12] B. Gulácsi and G. Burkard, Signatures of non-Markovianity of a superconducting qubit, *Phys. Rev. B* **107**, 174511 (2023).
- [13] A. P. Babu, T. Orell, V. Vadimov, W. Teixeira, M. Möttönen, and M. Silveri, Quantum error correction under numerically exact open-quantum-system dynamics, *Phys. Rev. Research* **5**, 043161 (2023).
- [14] M. Papič, A. Auer, and I. de Vega, Fast Estimation of Physical Error Contributions of Quantum Gates, [arXiv:2305.08916 \[quant-ph\]](https://arxiv.org/abs/2305.08916).
- [15] K. Nakamura and J. Ankerhold, Qubit dynamics beyond Lindblad: Non-Markovianity versus rotating wave approximation, *Phys. Rev. B* **109**, 014315 (2024).
- [16] K. Nakamura and J. Ankerhold, Gate Operations for Superconducting Qubits and Non-Markovianity, [arXiv:2402.18518 \[quant-ph\]](https://arxiv.org/abs/2402.18518).
- [17] J. Bylander, S. Gustavsson, F. Yan, F. Yoshihara, K. Harrabi, G. Fitch, D. G. Cory, Y. Nakamura, J.-S. Tsai, and W. D. Oliver, Noise spectroscopy through dynamical decoupling with a superconducting flux qubit, *Nat. Phys.* **7**, 565 (2011).
- [18] I. Almog, Y. Sagi, G. Gordon, G. Binsky, G. Kurizki, and N. Davidson, Direct measurement of the system-environment coupling as a tool for understanding decoherence and dynamical decoupling, *J. Phys. B: At. Mol. Opt. Phys.* **44**, 154006 (2011).
- [19] G. A. Álvarez and D. Suter, Measuring the Spectrum of Colored Noise by Dynamical Decoupling, *Phys. Rev. Lett.* **107**, 230501 (2011).
- [20] D. Ristè, C. C. Bultink, M. J. Tiggelman, R. N. Schouten, K. W. Lehnert, and L. DiCarlo, Millisecond charge-parity fluctuations and induced decoherence in a superconducting transmon qubit, *Nat. Commun.* **4**, 1913 (2013).
- [21] L. Cardani, F. Valenti, N. Casali, G. Catelani, T. Charpentier, M. Clemenza, I. Colantoni, A. Cruciani, G. D'Imperio, L. Gironi, *et al.*, Reducing the impact of radioactivity on quantum circuits in a deep-underground facility, *Nat. Commun.* **12**, 2733 (2021).
- [22] X. Pan, Y. Zhou, H. Yuan, L. Nie, W. Wei, L. Zhang,

- J. Li, S. Liu, Z. H. Jiang, G. Catelani, *et al.*, Engineering superconducting qubits to reduce quasiparticles and charge noise, *Nat. Commun.* **13**, 7196 (2022).
- [23] F. K. Wilhelm, S. Kirchhoff, S. Machnes, N. Wittler, and D. Sugny, An introduction into optimal control for quantum technologies, [arXiv:2003.10132 \[quant-ph\]](https://arxiv.org/abs/2003.10132).
- [24] R. Schmidt, A. Negretti, J. Ankerhold, T. Calarco, and J. T. Stockburger, Optimal Control of Open Quantum Systems: Cooperative Effects of Driving and Dissipation, *Phys. Rev. Lett.* **107**, 130404 (2011).
- [25] L. Viola and S. Lloyd, Dynamical suppression of decoherence in two-state quantum systems, *Phys. Rev. A* **58**, 2733 (1998).
- [26] H. Y. Carr and E. M. Purcell, Effects of Diffusion on Free Precession in Nuclear Magnetic Resonance Experiments, *Phys. Rev.* **94**, 630 (1954).
- [27] S. Meiboom and D. Gill, Modified Spin-Echo Method for Measuring Nuclear Relaxation Times, *Rev. Sci. Instrum.* **29**, 688 (1958).
- [28] E. L. Hahn, Spin Echoes, *Phys. Rev.* **80**, 580 (1950).
- [29] A. A. Maudsley, Modified Carr-Purcell-Meiboom-Gill sequence for NMR fourier imaging applications, *J. Magn. Reson.* **69**, 488 (1986).
- [30] G. T. Genov, D. Schraft, N. V. Vitanov, and T. Halfmann, Arbitrarily Accurate Pulse Sequences for Robust Dynamical Decoupling, *Phys. Rev. Lett.* **118**, 133202 (2017).
- [31] K. Khodjasteh and D. A. Lidar, Fault-Tolerant Quantum Dynamical Decoupling, *Phys. Rev. Lett.* **95**, 180501 (2005).
- [32] G. S. Uhrig, Keeping a Quantum Bit Alive by Optimized π -Pulse Sequences, *Phys. Rev. Lett.* **98**, 100504 (2007).
- [33] L. Viola and E. Knill, Robust Dynamical Decoupling of Quantum Systems with Bounded Controls, *Phys. Rev. Lett.* **90**, 037901 (2003).
- [34] A. M. Souza, G. A. Álvarez, and D. Suter, Robust Dynamical Decoupling for Quantum Computing and Quantum Memory, *Phys. Rev. Lett.* **106**, 240501 (2011).
- [35] L. Cywiński, R. M. Lutchyn, C. P. Nave, and S. Das Sarma, How to enhance dephasing time in superconducting qubits, *Phys. Rev. B* **77**, 174509 (2008).
- [36] J. Qi, X. Xu, D. Poletti, and H. K. Ng, Efficacy of noisy dynamical decoupling, *Phys. Rev. A* **107**, 032615 (2023).
- [37] B. Pokharel, N. Anand, B. Fortman, and D. A. Lidar, Demonstration of Fidelity Improvement Using Dynamical Decoupling with Superconducting Qubits, *Phys. Rev. Lett.* **121**, 220502 (2018).
- [38] N. Ezzell, B. Pokharel, L. Tewala, G. Quiroz, and D. A. Lidar, Dynamical decoupling for superconducting qubits: A performance survey, *Phys. Rev. Appl.* **20**, 064027 (2023).
- [39] M. J. Biercuk, H. Uys, A. P. VanDevender, N. Shiga, W. M. Itano, and J. J. Bollinger, Optimized dynamical decoupling in a model quantum memory, *Nature (London)* **458**, 996 (2009).
- [40] H. Uys, M. J. Biercuk, and J. J. Bollinger, Optimized Noise Filtration through Dynamical Decoupling, *Phys. Rev. Lett.* **103**, 040501 (2009).
- [41] A. Rahman, D. J. Egger, and C. Arenz, Learning How to Dynamically Decouple, [arXiv:2405.08689 \[quant-ph\]](https://arxiv.org/abs/2405.08689).
- [42] K. Shiokawa and D. A. Lidar, Dynamical decoupling using slow pulses: Efficient suppression of $1/f$ noise, *Phys. Rev. A* **69**, 030302(R) (2004).
- [43] L. I. Glazman and G. Catelani, Bogoliubov quasiparticles in superconducting qubits, *SciPost Phys. Lect. Notes* **31** (2021).
- [44] A. Blais, A. L. Grimsmo, S. M. Girvin, and A. Wallraff, Circuit quantum electrodynamics, *Rev. Mod. Phys.* **93**, 025005 (2021).
- [45] V. Tripathi, H. Chen, M. Khezri, K.-W. Yip, E. Levenson-Falk, and D. A. Lidar, Suppression of Crosstalk in Superconducting Qubits Using Dynamical Decoupling, *Phys. Rev. Appl.* **18**, 024068 (2022).
- [46] A. Barone and G. Paternò, *Physics and Applications of the Josephson Effect* (John Wiley & Sons, New York, 1982).
- [47] G. Wendin and V. S. Shumeiko, Superconducting Quantum Circuits, Qubits and Computing, [arXiv:cond-mat/0508729 \[cond-mat.supr-con\]](https://arxiv.org/abs/cond-mat/0508729).
- [48] G. Ithier, E. Collin, P. Joyez, P. J. Meeson, D. Vion, D. Esteve, F. Chiarello, A. Shnirman, Y. Makhlin, J. Schrieffer, *et al.*, Decoherence in a superconducting quantum bit circuit, *Phys. Rev. B* **72**, 134519 (2005).
- [49] S. Machlup, Noise in Semiconductors: Spectrum of a Two-Parameter Random Signal, *J. Appl. Phys.* **25**, 341 (1954).
- [50] E. Paladino, Y. M. Galperin, G. Falci, and B. L. Altshuler, $1/f$ noise: Implications for solid-state quantum information, *Rev. Mod. Phys.* **86**, 361 (2014).
- [51] C. Müller, J. H. Cole, and J. Lisenfeld, Towards understanding two-level-systems in amorphous solids: insights from quantum circuits, *Rep. Prog. Phys.* **82**, 124501 (2019).
- [52] M. Xu, Y. Yan, Q. Shi, J. Ankerhold, and J. T. Stockburger, Taming Quantum Noise for Efficient Low Temperature Simulations of Open Quantum Systems, *Phys. Rev. Lett.* **129**, 230601 (2022).
- [53] R. Kubo, M. Toda, and N. Hashitsume, *Statistical Physics II Nonequilibrium Statistical Mechanics* (Springer-Verlag, Berlin, 1985).
- [54] H.-P. Breuer and F. Petruccione, *The Theory of Open Quantum Systems* (Oxford University Press, Oxford, 2002).
- [55] A. G. Redfield, On the Theory of Relaxation Processes, *IBM J. Res. Dev.* **1**, 19 (1957).
- [56] G. Lindblad, On the generators of quantum dynamical semigroups, *Commun. Math. Phys.* **48**, 119 (1976).
- [57] Y. Tanimura, Stochastic Liouville, Langevin, Fokker-Planck, and Master Equation Approaches to Quantum Dissipative Systems, *J. Phys. Soc. Jpn.* **75**, 082001 (2006).
- [58] L. G. Rego, L. F. Santos, and V. S. Batista, Coherent Control of Quantum Dynamics with Sequences of Unitary Phase-Kick Pulses, *Annu. Rev. Phys. Chem.* **60**, 293 (2009).
- [59] P. Figueroa-Romero, M. Papič, A. Auer, M.-H. Hsieh, K. Modi, and I. de Vega, Operational Markovianization in randomized benchmarking, *Quantum Sci. Technol.* **9**, 035020 (2024).
- [60] D. Braun, F. Haake, and W. T. Strunz, Universality of Decoherence, *Phys. Rev. Lett.* **86**, 2913 (2001).
- [61] D. A. Lidar and T. A. Brun, *Quantum Error Correction* (Cambridge University Press, Cambridge, 2013).
- [62] L. Viola, E. Knill, and S. Lloyd, Dynamical Decoupling of Open Quantum Systems, *Phys. Rev. Lett.* **82**, 2417 (1999).
- [63] K. Khodjasteh and D. A. Lidar, Performance of deter-

ministic dynamical decoupling schemes: Concatenated and periodic pulse sequences, [Phys. Rev. A **75**, 062310 \(2007\)](#).

[64] R. P. Feynman, A. R. Hibbs, and D. F. Styer, *Quantum*

Mechanics and Path Integrals: Emended Editon (Dover Publications, Mineola, New York, 2017).